Astron. Astrophys. 315, 335–342 (1996)

ASTRONOMY AND ASTROPHYSICS

Infrared and visible coronal lines in NGC 1068*

A. Marconi[1], P.P. van der Werf[2], A.F.M. Moorwood[3], and E. Oliva[4]

[1] Dipartimento di Astronomia e Scienza dello Spazio, Università di Firenze, Largo E. Fermi 5, I-50125 Firenze, Italy
[2] Leiden Observatory, P.O. Box 9513, NL-2300 RA Leiden, The Netherlands
[3] European Southern Observatory, Karl Schwarzschild Str. 2, D-85748 Garching bei München, Germany
[4] Osservatorio Astrofisico di Arcetri, Largo E. Fermi 5, I-50125 Firenze, Italy

Received 19 January 1996 / Accepted 9 May 1996

Abstract. Infrared observations of [Si IX], [S IX] [Si VII], [Si VI], and [Ca VIII] coronal line emission in NGC 1068 are presented and discussed together with visible spectra covering [Fe VII], [Fe X], [Fe XI] and [S VIII]. These lines are found to peak $\simeq$ 50 pc NE of the nucleus and appear to arise predominantly in outflowing gas within the prominent ionization cone aligned with the radio jet. The line ratios argue against collisional ionization but could be explained with photoionization by radiation from the active nucleus. The observed [Si IX](3.935μm)/[Si VI](1.96μm) ratio is $\simeq 10^3$ larger than in NGC 6302, one of the highest excitation planetary nebulae known, demonstrating both that photoionization by hot stars is excluded and the potential value of the [SiIX](3.935μm) line as a tracer of AGN activity in visually obscured galactic nuclei.

Key words: line: formation – infrared: galaxies – galaxies: Seyferts – galaxies: individual: NGC 1068

1. Introduction

Coronal lines correspond to forbidden transitions within the ground terms of highly ionized species ($h\nu > 100$eV) which can be formed either in gas photoionized by a hard UV continuum (Grandi 1978, Korista & Ferland 1989) or in a hot ($\approx 10^6$ K) collisionally ionized plasma (Oke & Sargent 1969, Nussbaumer & Osterbrock 1970). Visible spectra of AGN contain the well known lines of [Fe VII], [Fe X], [Fe XI] and, sometimes, [Fe XIV] (361eV). The first infrared coronal line detected in a galaxy was [Si VI] λ1.963μm in NGC 1068 (Oliva & Moorwood 1990).

In a detailed study of the nearby (4Mpc) Circinus galaxy (Seyfert 2) Oliva et al. (1994, hereafter O94) observed a large set of coronal lines including new infrared detections and visible lines spanning a wide range of ionization potentials (100–400 eV). Based on modelling this large dataset they concluded in favour of photoionization and, from the line ratios, deduced the required shape of the ionizing continuum in the 100–400 eV range ($L_\nu \propto \nu^{-0.5}$) which turned out to be somewhat harder than that of typical Seyferts. Marconi et al. (1994a, hereafter M94) in a search for [Si VI] λ1.963μm in active galaxies found that the observed relation [Si VI]/[Fe VII]$\approx$1 also favours photoionization since collisional ionization (in e.g., shocks) tends to produce regions with [Si VI]/[Fe VII]$\ll$1.

In this paper we return to a more detailed discussion of NGC 1068 based on new infrared spectroscopy covering several coronal lines supplemented with visible archive data. NGC 1068 is of particular interest having been the prototype Seyfert 2 galaxy before becoming the paradigm for the unified Seyfert model following the detection of its broad line region in polarized light by Antonucci & Miller (1985). This model invokes the presence of a torus around the nucleus aligned such that the AGN and its broad line region are obscured along our line of sight (for a review see Antonucci 1993). The putative torus may also be responsible for collimating the radiation from the AGN, thus accounting for the pronounced ionization cone seen most clearly to the NE in [O III] λ5007 (Pogge 1989, Evans et al. 1991, Unger et al. 1992, Macchetto et al. 1994). The cone is rotated $\simeq$40° relative to the rotational axis of the galaxy, aligned with the pronounced radio jet (cf. Wilson & Ulvestad 1987) and most probably tilted slightly towards our line of sight (Cecil et al. 1990). Gas within it is presumably exposed directly to radiation from the AGN and, potentially, also to mass outflow driven by an AGN wind. To date, the highest excitation species studied in detail have been [OIII] (35 eV) (Alloin et al. 1983, Meaburn & Pedlar 1986) and [Ne V] (97 eV) (Bergeron et al. 1989) whose emission includes components consistent with photoionization within the cone. Here we extend such studies to the higher excitation coronal lines. In Sect. 4.1 we discuss positional and kinematic evidence that these lines arise predominantly within the ionization cone. In Sect. 4.2 we demonstrate that their line ratios are inconsistent with collisional ionization, exclude hot stars as the source of ionization by direct comparison with spectra of

Send offprint requests to: E. Oliva

* Based on observations collected at the European Southern Observatory, La Silla, Chile and data from the La Palma Data Archive.

Table 1. Parameters of archival data.

Wavelength (Å)	Observation Date	Slit	Standard Star
3400 – 5100	3 September 1990	1.″4	HD 19445
3400 – 5100	3 September 1990	5.″4	HD 19445
4800 – 5600	6 January 1988	1.″5	40 ERI B
5600 – 6800	30 August 1990	1.″5	HD 19445
7800 – 9300	24 November 1986	1.″5	HD 84937
9600 – 10300	13 January 1987	2.″2	Feige 25

a high excitation planetary nebula and conclude that photoionization by an AGN spectrum is the most likely mechanism. Our overall conclusions are given in Sect. 5.

2. Observations and data reduction

The infrared data were collected in November 1994 using the ESO long slit spectrometer IRSPEC (Moorwood et al. 1991) mounted on the ESO–NTT telescope. The detector was an SBRC 62x58 InSb array with projected pixel size of 2.″2 along the slit and $\simeq$ 2 Å at 1.25μm, $\simeq$ 5 Å at 2.2μm, $\simeq$ 10 Å at 4μm along the dispersion. The slit width was 4.″4 (2 pixels) yielding a resolving power of R = 2000 – 3000 depending on wavelength. The observations consisted of several pairs of object and sky frames spaced by 2 minutes and with the slit aligned along the axis of the ionization cone at PA 31°. On chip integration time was 60 sec at $\lambda < 2.5\mu$m and 0.6 sec at 4μm. The data were reduced using the IRSPEC context in the ESO reduction package MIDAS. The spectra were wavelength calibrated using OH sky lines (at $\lambda < 2.3$ μm, Oliva & Origlia 1992) or a neon lamp and corrected for atmospheric and instrumental transmission using measurements of featureless, early O stars. Absolute flux calibration was derived from observations of photometric standard stars.

Archival raw optical spectral data were collected from the La Palma Archive (Zuiderwijk et al. 1994) and consisted of object, lamp and standard star frames taken with the Intermediate Dispersion Spectrograph (IDS) on the 2.5m Isaac Newton Telescope (INT; for more information see Table 1). When recorded, slit orientations were in the range PA 37-40° i.e close to the axis of the ionization cone. Data reduction was performed using standard procedures for long–slit CCD spectra and wavelength calibration was optimized using sky emission lines (Osterbrock & Martel 1992).

The use of slightly different slit angles and sizes for IR and optical observations should not affect the results presented in this paper where our main interest is the coronal line emission which is concentrated towards the nucleus and less extended than the slit.

Table 2. Observed and dereddened line fluxes.

Line	F_{-14} [1]	I_{-14} [2]	Other Data
IR Observations (λ in μm):			
[Fe II] λ1.2567	50	58	39[a]
[S IX] λ1.25235*	5	6	
H_2 λ1.9570	15	16	15[a]
[Si VI] λ1.963	70	75	75[a]
[Si VII] λ2.483	55[b]	58	90[c]
[Ca VIII] λ2.321	45	47	
[Si IX] λ3.9346*	46	47	
Optical observations (λ in Å):			
[Ne V] λ3426	93	230	
" (wide slit)	270	670	168[d]; 115[e]
[S II]+Hδ	29	65	
" (wide slit)	72	160	70[d]; 59[e]
He II λ4686	25	52	
" (wide slit)	50	101	60[d]; 61[e]
Hβ	67	132	
" (wide slit)	140	280	145[d]; 160[e]
[O III]	1370	2620	
" (wide slit)	2900	5540	2280[d]; 2800[e]
[Fe XIV] λ5303	<10	<20	
[Ca V] λ5309	<10	<20	
[Fe VII] λ6087	27	63	35[d]; 35[e]
[O I] λ6300	53	86	80[d]; 99[e]
[OI]+[FeX]	24	39	20[d]; 46[e]
[Fe X] λ6374	6	10	<10[d]; 7.5[e]
Hα+[NII]	1600	2540	2110[d]; 2420[e]
[S II] λ6720	160	251	190[d]; 235[e]
[Fe XI] λ7892	6.6	9.4	
[S III] λ9052	186	245	170[d]
[C I] λ9850	9.3	12	30[d]
[S VIII] λ9912	8.7	11	
HeII λ10124	27[f]	34[f]	25[d]

[1] Observed line flux in units of 10^{-14} erg cm^{-2} sec^{-1}.
[2] Dereddened flux (same units) adopting E(B-V)=0.2
* Rest wavelengths of [Si IX] and [S IX] from O94.
[a] Observed flux from Oliva & Moorwood 1990.
[b] Flux is very uncertain due to bad atmospheric transmission.
[c] Observed flux from Moorwood & Oliva 1991.
[d] Observed flux from Shields & Oke 1975 (7" ⊘ diaphragm).
[e] Observed flux from Koski 1978 (2.7"x4.0" aperture).
[f] Very uncertain (end of CCD sensitivity).

3. Results

The infrared spectra are displayed in Fig. 1 and the observed line fluxes are listed in Table 2. The [S IX] and [Si IX] lines are new discoveries in this object and, thanks to the excellent atmospheric transmission at their wavelengths, are measured at high signal to noise ratio. Fluxes of other lines are in good agreement with previous measurements (Oliva & Moorwood 1990) except for [Si VII] which lies in a region of very poor atmospheric transmission and which we find ≈30% fainter than in the lower S/N spectrum of Moorwood & Oliva (1991).

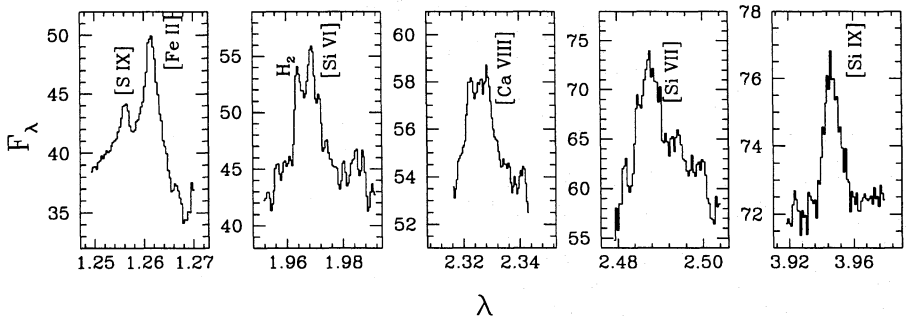

Fig. 1. IRSPEC spectra at selected grating positions around coronal lines. Flux F_λ is in units of 10^{-11} erg cm^{-2} s^{-1} μm^{-1} and wavelengths are in μm.

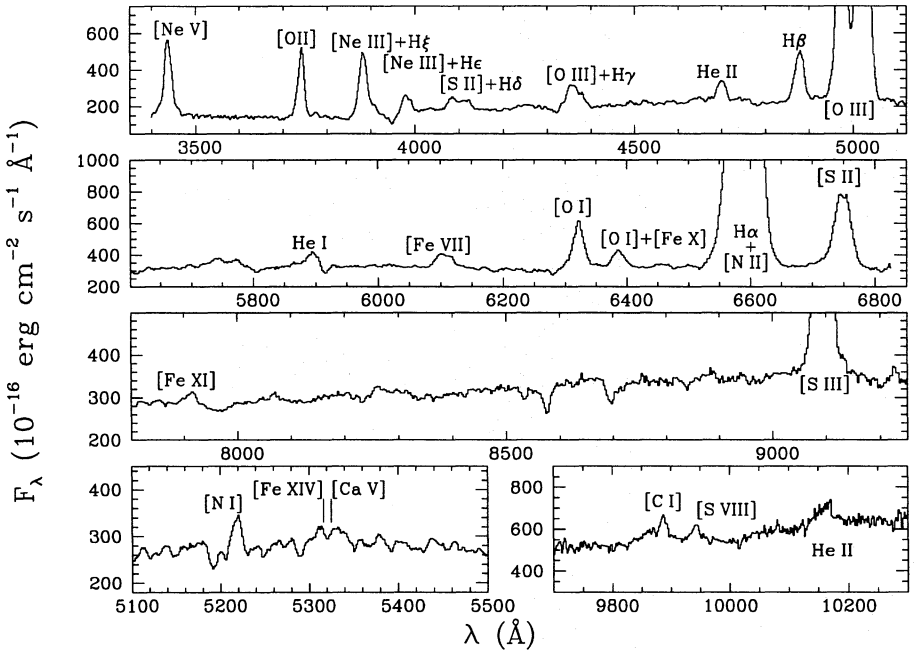

Fig. 2. Selected parts of the optical spectra. The expected positions of [Fe XIV] λ5303 and [Ca V] λ5309 (neither detected, see also Fig. 3) are marked. Note the complicate structure of stellar lines in the underlying continuum.

The optical spectra are displayed in Fig. 2 and the observed line fluxes are listed in Table 2 which also includes data from the literature for comparison. When overlap exists our fluxes are in good agreement with previous measurements taking into account the effect of the different slit sizes. Most of our line ratios are also in reasonable agreement with the very recent work by Osterbrock and Fulbright (1995) whose uncalibrated spectra also cover the far red region.

The coronal lines have relatively low line/continuum ratios (<10%) and measurements are therefore complicated by contamination from the strong stellar absorption features. However, as shown in Fig. 3 this stellar continuum can be adequately removed by subtracting a rescaled spectrum of the region ≈5″above and/or below the nucleus. The [Fe X] λ6374 line is blended with [O I] λ6363 and the deblending was performed with a gaussian fit where FWHM, amplitude and center wavelength for the latter are inferred from the [O I] λ6300 line (which arises from the same upper level as [O I] λ6363). [Fe XIV] λ5303 and [Ca V] λ5309 are not detected and the origin of the broad ($\simeq$ 4000 km s^{-1}) feature which appears at ≃5300Å (lower left panel of Fig. 3) is unclear. We conservatively take a 10% line/continuum ratio as un upper limit for these lines.

The heliocentric velocities derived from gaussian centroids of IR and visible lines are plotted in Fig. 4 and listed in Table 3 together with the FWHM of selected lines detected with sufficient S/N and affected least by blending. Most line centroids are blueshifted relative to the systemic velocity (the dashed line of Fig. 4).

Fig. 4 indicates a different behaviour according to the ionization potential: low excitation lines (i.e. $E < 20$ eV) with a mean centroid velocity of $\simeq$ 1080 km s^{-1}; medium excitation species ($20 < E < 100$ eV) with a mean centroid velocity of $\simeq$ 930 km s^{-1} and the coronal lines ($E > 100$ eV) with a mean centroid velocity of $\simeq$ 850 km s^{-1}. Any trend of the FWHM with ionization potential is less clear except that those of the medium excitation species appear to be larger than those of lower (forbidden but not HI) and higher ionization potential.

Fig. 5 shows position–velocity contour plots for selected visible lines. All show a broad component extending several arcsec along the slit plus a narrower component near to the systemic velocity further out. The line emission peaks are blueshifted and (except for [Ne V]) displaced $\simeq$ 0.″6 NE of the optical contin-

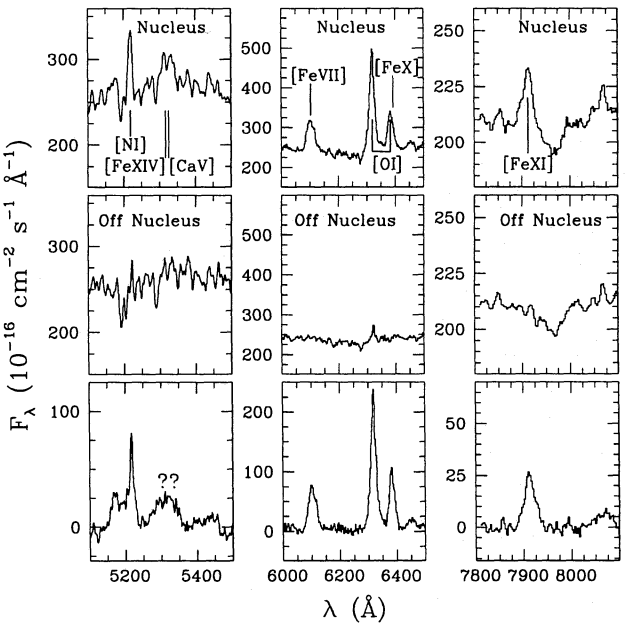

Fig. 3. Upper and central panels: nuclear and rescaled extra–nuclear spectra around lines of interest. Lower panels: difference between the above spectra. Note that the stellar absorption features almost disappear. The expected positions of [Fe XIV] λ5303 and [Ca V] λ5309 (neither detected) are also marked; the origin of the broad feature at ≃5300 Å is unclear.

uum. Definitive statements on the peak positions of the higher excitation visible lines are difficult because of blending and low S/N ratio. Although our infrared spectra were obtained with ≃ 2″pixels the infrared coronal lines also appear to be displaced ≃ 0.″5 NE of the continuum and to extend over ≤ 4″. Both [O III] and He II also show a velocity gradient across the nucleus which is more pronounced in the higher excitation [Ne V] and [Fe VII] lines but virtually absent in the low excitation [O I] and Hβ lines and will be discussed further below.

The presence of a broad and a narrow component in [O III] and Hβ was already shown in a detailed profile analysis by Alloin et al. (1983) who identified two main components, namely blueshifted broad lines at ≃895 km s^{-1} and narrower features closer to the systemic velocity, and this is consistent with what we find here. The relative importance of these two components determines the position of the line centroids of Fig. 4. As it is, high excitation (coronal) lines weight more the broad, blue component while lower ionization features are dominated by the redder component.

The blueshift of the broad component cannot be due to selective extinction, since high excitation lines with very different wavelengths show the same velocities. It is likely due to gas outflows from the nucleus which were already reported in the literature (see Sect. 4.1 for more details). Therefore, coronal lines are mainly emitted by outflowing material while for intermediate excitation lines such as [O III] there is a combination of outflowing and rotating material.

Table 3. Heliocentric velocities of IR and optical lines.

Line	Energy[a]	Heliocen. Vel.[b]	FWHM[b]
H_2 (3,0) λ1.957	–	1100 ±50	–
[N I] λ5200	–	1040 ±50	–
[C I] λ9850	–	1070 ±50	–
[Fe II] λ1.257	7.9	1140 ±50	1070
Hβ λ4861	13.6	1030 ±30	1500
[S III] λ9069	23.3	925 ±30	–
He I λ5876	24.6	950 ±50	–
[O III] λ5007	35.1	935 ±30	1400
He II λ4686	54.4	915 ±30	1640
[Fe VII] λ6087	100	840 ±50	1640
[Si VI] λ1.963	167	870 ±50	–
[Fe XI] λ7892	262	810 ±50	950
[S VIII] λ9913	280	850 ±50	–
[Si IX] λ3.935[c]	303	880 ±50	1000
[S IX] λ1.252[c]	328	870 ±50	–

[a] Energy needed to produce the species (eV).
[b] Units of km s^{-1}.
[c] Rest wavelength of [Si IX] and [S IX] from O94.

4. Discussion

4.1. Location and kinematics of the coronal line region.

The evidence presented above indicates that the visible and infrared lines peak within the ionization cone to the NE and at ≃ 0.″5 (≃ 50pc) from the nucleus. The exception which we cannot account for is [Ne V] which does not appear to be displaced from the nucleus in the archive spectra used here. For [O III] in particular, both the displacement of the line peak and the overall positional dependence of the line profiles are in accord with previous studies made at higher spectral resolution (Alloin et al. 1983, Meaburn & Pedlar 1986). In addition, however, the higher resolution spectra show splitting of the broad component on both sides of the nucleus indicative of gas flowing in opposed hollow cones (Meaburn & Pedlar 1986). This line splitting is also present in [N II] Fabry-Perot spectral images obtained by Cecil et al. (1990) and modelled by them as an outflow with velocity of ≃1500 km s^{-1} within a cone whose axis, inferred from the velocity asymmetry, is inclined 75° to our line of sight. This model assumed the cone opening angle of 82° deduced by Bergeron et al. (1989) from their detection of extended [Ne V] emission away from the nucleus along slits located on either side. The cone is better defined in the [O III] images of Unger et al. (1992) and has a smaller opening angle of 40°. Following Cecil et al. but assuming the smaller [O III] cone opening angle and the velocity components at $-810, 295$ km s^{-1} from Meaburn & Pedlar (1986) yields a somewhat larger inclination angle ≃80° and outflow velocity in the cone.

From the above we conclude that [O III] comprises a component associated with outflow gas in the ionization cone(s), whose NE lobe is tilted towards our line of sight, and that this accounts for the velocity gradient across the nucleus evident in Fig. 5. The fact that this gradient is virtually absent in the plots

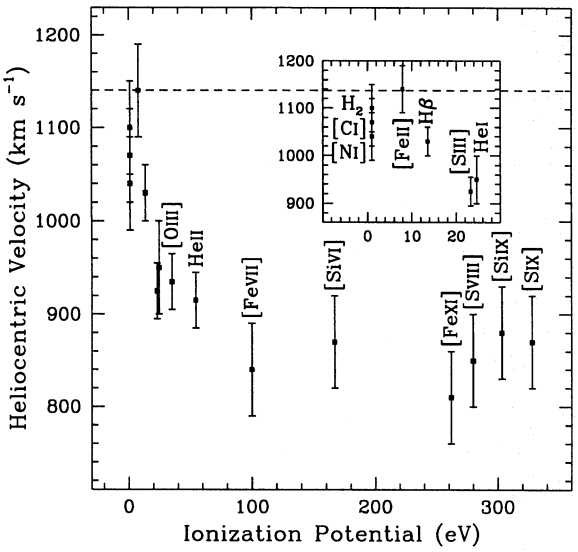

Fig. 4. Heliocentric velocities from gaussian centroids of IR and optical lines. The dashed line is the systemic velocity from HI measurements (Baan & Haschick 1983). The small panel is an enlargement for low ionization species.

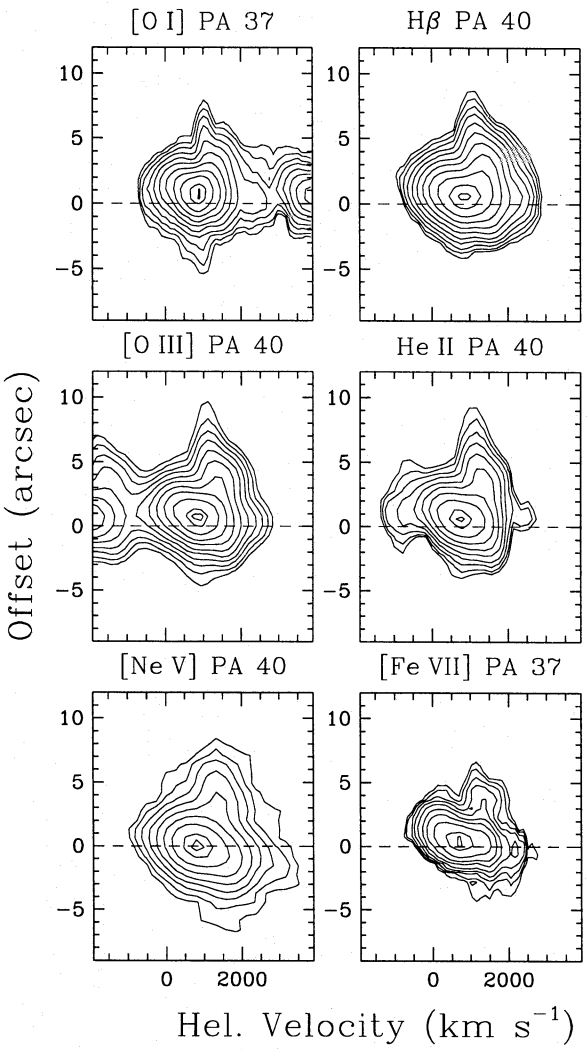

Fig. 5. Intensity contour plots in the position–velocity plane for selected visible lines. The ordinate gives the relative position along the slit whose PA is indicated at the top of each plot (i.e. NE is up). A null offset gives the centroid of continuum emission along the slit. Contours are logarithmically spaced by 0.2 dex from 1% to 100% of the peak but are only included at the lowest levels when above the noise. The absolute velocity scale for [Ne V] is not reliable since the line is at the very edge of the detector.

of the low excitation lines [O I] and Hβ and more pronounced in the plots of the higher ionization potential ($\simeq$100eV) species [Ne V] and [Fe VII] can therefore be interpreted naturally as an increase in the cone component with increasing excitation. Although we do not have position–velocity maps for all of the higher excitation lines, Fig. 4 shows that their velocity centroids are identical within the errors but $\simeq$100 km s^{-1} bluer than the medium excitation and $\simeq$ 300 km s^{-1} bluer than the low excitation lines and the systemic velocity. The fact that lines with similar ionization potentials but sometimes widely different wavelengths (e.g [S III] λ9069 and He II λ4686; [Fe XI] λ7892 and [SiIX] 3.935 μm) show similar heliocentric velocities provides additional evidence that the observed kinematics is related to non-isotropic flows and/or ionization structure rather than selective extinction effects. The smaller FWHM and larger blueshifts of the high ionization potential lines compared with the medium excitation species in Table 3 suggests that they may arise in a more restricted part of the flow, possibly closer to its axis and/or apex. Overall, therefore, the situation in NGC 1068 is similar to that observed in other AGN's and, in particular, to that in the Circinus galaxy where the coronal lines are blueshifted by $\simeq$50 km s^{-1} relative to [O III] (O94) and, based on [FeXI], arise closer to the nucleus within the apex of the ionization cone (Marconi et al. 1994b). In Circinus, as in NGC 1068, the blueshift cannot be due to extinction since it is independent of wavelength.

4.2. Ionization mechanism of the Coronal Line Region

4.2.1. Collisional ionization

As the coronal lines appear to arise in outflowing gas which is probably driven by an AGN wind (cf. Smith 1983) we first test if they could be produced in a collisionally ionized plasma heated by a fast shock wave ($v > 300$ km s^{-1}). Under the simplifying assumption that any contribution from photoionization is negligible, the ionization state of the gas follows from statistical equilibrium between collisional ionization and radiative plus dielectronic recombination, and is solely determined by the gas temperature T (e.g. Jordan 1969). Values of $x(X^{+i})$ (the ionization fraction of a given species X^{+i}) as a function of T have been computed and tabulated in the above reference and subsequently updated by various authors. We adopt here the most recent results of Monsignori Fossi & Landini (1996) which are plotted in the bottom panels of Fig. 6.

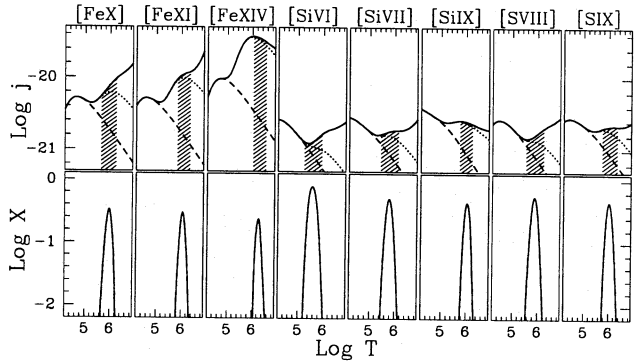

Fig. 6. Lower panels: variation of the ionization fraction as a function temperature in a collisionally ionized gas. Upper panels: line emission coefficients (erg cm^3 s^{-1}) including only direct electron excitation (dashed lines), adding indirect electron excitation (dotted lines) and including also proton collisions (solid lines), the adopted atomic parameters are described in Sect. 4.3 of O94. The dashed areas show the temperature range where the ionic fraction is larger than 10^{-2}.

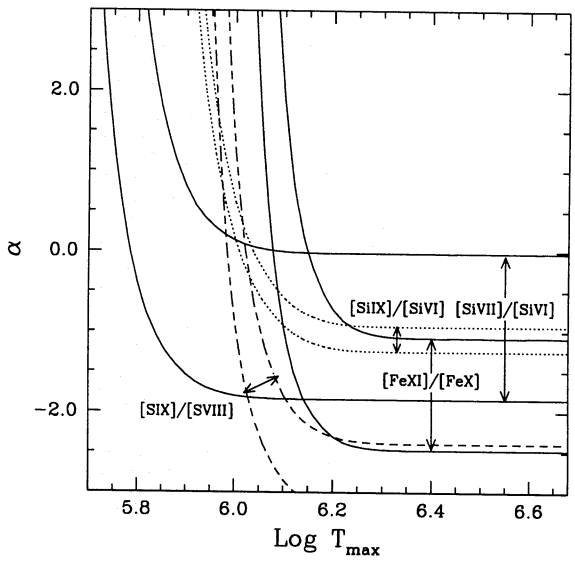

Fig. 7. Predicted line ratios from a model of hot, collisionally ionized gas as a function of T_{max} (upper cut in temperature for the gas distribution) and α (the slope of temperature distribution). The curves show the loci compatible, within the errors, with the observed line ratios. There is no combination of $T_{\rm max}$ and α which can reproduce the observations (see Sect. 4.2.1).

In a hot, collisionally ionized gas the kinetic energy of electrons and protons is comparable to $h\nu_{\rm ion}$, the ionization potential of a given ion. Consequently, the line formation is dominated by direct proton collisions to "u" (the upper level of the observed transition) and electron excitations of high lying states which cascade to "u". The relative contributions of these processes are visualized in the upper panels of Fig. 6 which show the emission coefficients for the lines of interest including all processes (solid lines), excluding proton collisions (dotted lines) and including only direct electron excitations (dashed lines). The most striking result is that the emissivity of Fe ions (expecially [Fe XIV]) is strongly enhanced by electron collisions of their numerous high lying states, while in other species the effect is much smaller. A collisionally ionized gas should be therefore characterized by large [Fe]/[Si] and [Fe]/[S] line ratios, and the brightest line should be [Fe XIV]λ5303 unless the temperature is kept well below 2 10^6 K. i.e. the temperature at which most of iron is in the form of FeXIV (cf. Fig. 6).

A single component model where all the gas is at a single temperature is unrealistic and cannot reproduce the observed wide range of ionization stages. Similarly to Nussbaumer & Osterbrock (1970) we assume therefore that the lines originate in regions with different temperatures and with volume emission measures $EM = n_e^2 V$ (n_e is the electron density and V is the volume occupied) distributed according to a power law, $EM(T) \propto T^{\alpha}$, cut at $T_{\rm min}$ and $T_{\rm max}$. We also assume that the density of the plasma is lower than the critical densities for collisional excitation of the transitions considered, i.e. $n_e \leq 10^8\,{\rm cm}^{-3}$. Using the function plotted in Fig. 6 we constructed a grid of models at different α, $T_{\rm min}$ and $T_{\rm max}$ with the following results:

- the choice of $T_{\rm min}$ has little influence on the lines considered here.
- the ratio [Si VI]/[Si VII] depends primarily on α, the observed value indicating $-2 < \alpha < 0$.
- [Si IX]/[Si VI], [S IX]/[S VIII], [Fe XI]/[Fe X] and [Fe XIV]/[Fe XI] critically depend on the choice of $T_{\rm max}$: changing the upper temperature cutoff by only 0.2dex produces a factor $\geq$2 variation of these line ratios, and for $T_{\rm max} > 2 \cdot 10^6$ K too much [Fe XIV] is predicted.

These considerations are summarized in Fig. 7 which shows the loci of the $T_{\rm max}$–α plane compatible with the observed line ratios. Note that the ratios of higher excitation lines cannot be simultaneously reproduced with any combination of parameters, indicating that the model is unrealistic. Moreover, the predicted [Fe]/[S] ratios are a factor of $\sim$3 higher than those observed for the reasons given above. We note furthermore that the [Si VI]/[Fe VII] ratio of 1.19$\pm$0.24, is characteristic of photoionization and much larger than in shocks (cf. M94 and Sect. 1). Finally, although the lines in NGC 1068 are broad, we recall that shock heating is effectively excluded in the case of the Circinus galaxy by the small width of its coronal lines ($<$ 100 km s^{-1}; O94). Therefore, while some contribution from shocks or X–rays emitted by a shock front cannot be excluded, the above arguments suggest that the coronal line gas in NGC 1068 is predominantly photoionized.

4.2.2. Photoionization

Fig. 8 demonstrates, totally independent of model assumptions, that the [Si IX] observed in NGC 1068 cannot arise in gas photoionized by hot stars. Whereas both NGC 1068 and the Circinus galaxy exhibit comparable fluxes in the [Si VI],[Si VII] and [Si IX] lines, [Si IX] is absent in our spectrum of NGC 6302,

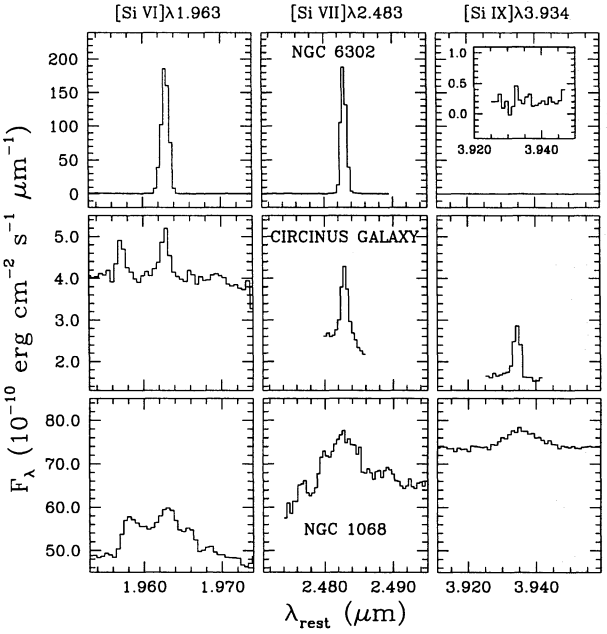

Fig. 8. The [Si VI], [Si VII] and [Si IX] lines of the planetary nebula NGC 6302 and of the Seyfert 2 galaxies Circinus and NGC 1068. Fluxes per unit wavelength have been multiplied by the reddening correction at the wavelength of the lines (A_V = 2.5 for NGC 6302, A_V = 5.2 for Circinus and A_V = 0.62 for NGC 1068).

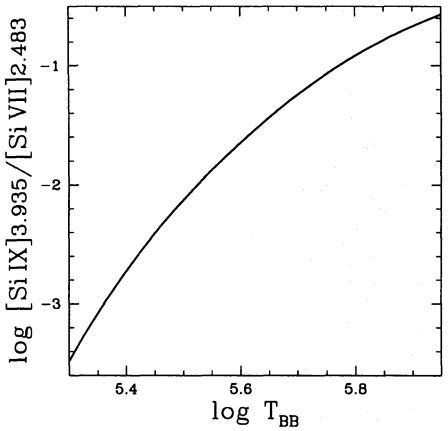

Fig. 9. Predicted variation of [Si IX]/[Si VII] for a spherical nebula photoionized by a blackbody with temperature T_{BB}.

amongst the highest excitation planetary nebulae known, to a limit [Si IX]/[Si VII]<2× 10^{-3}.

The predicted value of [Si IX]/[Si VII] for a spherical nebula photoionized by a black body with temperature $T_{\rm BB}$ is plotted in Fig. 9. Data are based on photoionization models computed with Cloudy (version 84.06, Ferland 1993) and adopting distorted–wave collision strengths from the compilation by Kafatos & Linch (1980). Results are accurately reproduced by the simple interpolation formula

$$\frac{[\mathrm{Si\,IX}]}{[\mathrm{Si\,VII}]} = 1.7\, e^{-1.76/T_6} \quad ; \quad T_6 = T_{\rm BB}/10^6\ \mathrm{K} \qquad (1)$$

Table 4. Reddening corrected ratios of coronal lines.

Ratio	Energy [a]		Circinus[b] 1.68[c]	NGC 1068 0.20[c]
[Fe VII]/[Fe X]	100	235	0.47 ±0.08	6.30 ±0.90
[Fe XI]/[Fe X]	262	235	0.65 ±0.10	0.94 ±0.14
[S IX]/[S VIII]	328	280	0.96 ±0.15	0.55 ±0.08
[Si VII]/[Si VI]	206	167	1.61 ±0.24	0.77 ±0.30
[Si IX]/[Si VI]	303	167	2.12 ±0.32	0.63 ±0.10
[Si VI]/[Fe VII]	167	100	1.60 ±0.24	1.19 ±0.24
HeII/Hβ	54.4	13.6	0.30 ±0.05	0.39 ±0.04

[a] Energy needed to produce the ions (eV).
[b] From O94
[c] Adopted E(B-V) for reddening correction.

and have general validity as long as the nebula is radiation bounded and the ionization structure of the two species is dominated by geometric dilution, i.e. for $\Xi = Q(\mathrm{He}^+)\, n_e\, f^2 \lesssim 10^{53}$ cm^{-3} s^{-1} [here $Q(\mathrm{He}^+)$ is the He^+ ionizing photon rate in s^{-1}, n_e is the electron density and f is the filling factor]. At larger values of Ξ the ionization strucure of [Si VII] is 'cut' by He^+ continuum opacity and the ratio [Si IX]/[Si VII] slightly increases (the definition of Ξ and a detailed discussion of the relative roles of geometric dilution and continuum opacity in spherical nebulae can be found in Sect. 4.1.1 of M94). It is found from Fig. 9 that the star ionizing NGC 6302 has $T_{\rm BB} \lesssim 2.5\times 10^5$ K and that [Si IX]/[Si VII] ratios similar to those observed in Seyferts require $T_{\rm BB} \gtrsim 10^6$ K. The [Si IX] (3.935μm) line thus appears to be an ideal tracer of AGN activity in galaxy nuclei including, because of its relatively long infrared wavelength, those which are obscured in the visible.

Having excluded collisional ionization and photoionization by hot stars, photoionization by radiation from the AGN is clearly the most likely source of excitation of the coronal lines in NGC 1068. Detailed confirmation by modelling would require more information on the size and physical conditions of the emitting regions which is not available here. Referring to the line ratios in Table 4, NGC 1068 has a somewhat lower ionization CLR since all high to low excitation line ratios are smaller than in Circinus except for [Fe XI]/[Fe X] and with the most striking differences being [Fe VII]/[Fe X] and [Si IX]/[Si VI]. This might either indicate a steeper ionizing continuum or a somewhat lower ionization parameter in NGC 1068.

5. Conclusions

Infrared spectra of the [Ca VIII], [Si VI], [Si VII], [Si IX] and [S IX] coronal lines in the prototype Seyfert 2 galaxy NGC 1068 have been presented and discussed together with La Palma archive spectra of the visible [Fe VII], [Fe X], [Fe XI] and [S VIII] coronal plus lower excitation lines. The [S IX](1.252μm) and [Si IX](3.935μm) infrared lines are new detections in this galaxy.

Both the visible and infrared coronal lines exhibit the same blueshift relative to lower excitation species and the systemic velocity which is indicative of non-isotropic velocity flows rather than e.g selective extinction. This is supported by position–velocity intensity contours of selected visible lines which are consistent with extended emission over $\simeq$300 pc and an increase with ionization potential of the fraction associated with outflowing gas within the well known ionization cones aligned with radio jets to the NE and SW of the nucleus. Coronal lines appear to peak $\simeq 0''.5$ NE of the nucleus i.e close to the position found for [O III] here and in previous studies.

The coronal line ratios argue against collisional ionization but can be produced in gas photoionized by radiation from the active nucleus. Although detailed modelling is not possible here the ionizing continuum must, nevertheless, be much harder than that of hot stars. The observed [Si IX]/[Si VI] ratio is $\simeq 10^3$ larger than in NGC 6302, one of the highest excitation planetary nebulae known. This not only excludes stellar photoionization but also underlines the potential of the [Si IX](3.935μm) line as a tracer of AGN activity in visually obscured galactic nuclei.

Acknowledgements. We are grateful to the staff on La Palma for their effort in providing us with the visible archive spectra. The Isaac Newton Telescope is operated on the Island of La Palma by the Royal Greenwich Observatory in the Spanish Observatory del Roque de los Muchachos of the Instituto de Astrofisica de Canarias. This research has made use of the NASA/IPAC Extragalactic Database (NED) which is operated by the Jet Propulsion Laboratory, California Institute of Technology, under contract with the National Aeronautics and Space Administration. We thank D. Osterbrock for showing us his 7000–10900 Å spectrum of NGC 1068 before pubblication. We thank Gary Ferland for making available his photoionization code Cloudy. The research of Van der Werf has been made possible by a fellowship of the Royal Netherlands Academy of Arts and Sciences. We thank Dr. Hagai Netzer, the referee, for useful discussions and suggestions which improved this paper.

References

Alloin D., Pelat D., Boksenberg A., and Sargent W.L.W., 1983, ApJ 275, 493
Antonucci R.R.J. and Miller J.S., 1985, ApJ 297, 621
Antonucci R.R.J., 1993, ARA&A 31, 473
Baan W.A., Haschick A.D., 1983, AJ 88, 1088
Bergeron J., Petitjean P., and Durret, F., 1989, A&A 213, 61
Cecil G., Bland J., and Tully R.B.,1990, ApJ 355, 70
Evans I.N., Ford H.C., Kinney A.L., Antonucci R.R.J., Armus L., and Caganoff S., 1991, ApJ 369, L27
Ferland G.J., 1993, University of Kentucky Department of Physics and Astronomy Internal Report
Grandi S.A., 1978, ApJ 221, 501
Kafatos M. and Lynch J.P., 1980, ApJS 42, 611
Korista K.T., Ferland G.J., 1989, ApJ 343, 678
Koski A.T., 1978, ApJ 223, 56
Jordan C., 1969, MNRAS 142, 501
Marconi A., Moorwood A.F.M., Salvati M. and Oliva E., 1994a, A&A 291, 18 (M94)
Marconi A., Moorwood A.F.M., Origlia L., and Oliva E., 1994b, The Messenger 78, 20
Macchetto F., Capetti A., Sparks W.B., Axon D.J., and Boksenberg A., 1994, ApJL 435, L15
Meaburn J., Pedlar A., 1986, A&A 159, 336
Monsignori Fossi B. and Landini M., 1996, *Astrophysics in the Extreme UV*, ed. S. Bowyer, R.F. Malina, p. 543
Moorwood A.F.M., Moneti A., Gredel R., 1991, The Messenger 63, 77
Moorwood A.F.M. and Oliva E., 1991, The Messenger 63, 57
Nussbaumer H. and Osterbrock D.E., 1970, ApJ 161, 811
Oliva E. and Moorwood A.F.M., 1990, ApJ 348, L5
Oliva E. and Origlia L., 1992, A&A 254, 466
Oliva E., Salvati M., Moorwood A.F.M. and Marconi A., 1994, A&A 288, 457 (O94)
Oke J.B. and Sargent W.L.W., 1969, ApJ 151, 807
Osterbrock D.E. and Martel A., 1992, PASP 104, 76
Osterbrock D.E. and Fulbright J.P., 1996, PASP 108, 183
Pogge R.W., 1989, ApJ 345, 730
Shields G.A. and Oke J.B., 1975, ApJ 197, 5
Smith S.J., 1993, ApJ 411, 570
Unger S.W., Lewis J.R., Pedlar A., and Axon D.J., 1992, MNRAS 258, 371
Wilson A., Ulvestad J.S., 1987, ApJ 319, 105
Zuiderwijk E.J., Martin R., Raimond E., and van Diepen G.N.J., 1994, PASP 106, 515

This article was processed by the author using Springer-Verlag LaTeX A&A style file *L-AA* version 3.